Experimental Testing of Continious Control Set Model Predictive Control for Three-phase Voltage Source Converters

Mardani, Mohammad Mehdi; Mijatovic, Nenad; Rodriguez, José ; Dragicevic, Tomislav

Published in:
Proceedings of 6th IEEE International Conference on Predictive Control of Electrical Drives and Power Electronics

Link to article, DOI:
10.1109/PRECEDE51386.2021.9681024

Publication date:
2023

Document Version
Peer reviewed version

Experimental Testing of Continious Control Set Model Predictive Control for Three-phase Voltage Source Converters

Mohammad Mehdi Mardani
Department of Electrical Engineering Electronics,
Technical University of Denmark,
2800 Kgs. Lyngby, Denmark.
e-mail: mmema@elektro.dtu.dk

Sino-Danish College (SDC), University of Chinese Academy of Sciences

Nenad Mijatovic
Department of Electrical Engineering Electronics,
Technical University of Denmark,
2800 Kgs. Lyngby, Denmark.
e-mail: nm@elektro.dtu.dk

Tomislav Dragicevic
Department of Electrical Engineering Electronics,
Technical University of Denmark,
2800 Kgs. Lyngby, Denmark.
e-mail: tomdr@elektro.dtu.dk

Jose Rodriguez
Faculty of Engineering,
Universidad Andres Bello,
Santiago 8370146, Chile.
e-mail: jose.rodriguez@unab.cl

***Abstract*—Grid-connected voltage source converters (VSCs), which are the key block of the future power electronics-based power systems, are at a high risk of losing stability and robust performance. These challenges in industrial applications require analyzing and designing a simple, robust, and advanced controller to guarantee not only reliable operation but also the performance of the VSCs. This paper proposes a novel constraint and unconstraint continuous control set (CCS) model predictive controller (MPC) for VSCs. In the unconstraint MPC, the optimal control law is analytically calculated. However, for the constraint MPC, the analytical solution is not available. So, the convex optimization methods are used to find the suboptimal solution. Generally, the key novelties of this paper can be enumerated as using CCS-MPC to obtain fixed switching frequency, considering hard constraints on the amplitude of the input and output signals, and analytically obtain the optimal solution for unconstraint MPC. Finally, to evaluate the validity of the proposed approaches, some experimental tests on the laboratory-scale stand-alone VSC are extracted.**

Keywords—Grid connected voltage source converter (VSC), continuous control set (CCS) model predictive controller (MPC), hard constraints, optimal control, experimental test

I. INTRODUCTION

Increasing electricity demand results in the world's ambitious target for harvesting maximum energy from renewable energy sources (RESs) in the coming decade. Thus, the trend of designing and connecting a high amount of renewable energy sources (RESs) to electrical power grids is intensified. Three-phase voltage source converters (VSCs) are vital intermittent equipment to connect RESs like photovoltaics (PVs) and wind turbines (WTs) to the grid [1], [2]. However, one of the challenging issues with VSCs is designing a controller to improve the performance of hybrid power plants (HPPs) [3].

One of the conventional control approaches for voltage source converters (VSC) is using a vector current control (VCC). In the VCC, the synchronous rotating reference frame and coordinate transfer are used to transfer ac signals to the dc one [4]. Then, the VSC can be described in a linear time-invariant (LTI) system, which is suitable for implementing linear control theories. In this structure, proportional-integrator (PI) and proportional-resonant (PR) controllers are the most common approaches to control active and reactive currents [5], [6]. However, the main drawbacks of the linear controllers are their sluggish transient response, their applicability only around a small vacancy of the equilibrium point, and their sensitivity to control gain matrices. To improve the transient response of the VSCs, the direct-power control (DPC) method is presented [4], [7]. The common approach in DPC is using a lookup table [8]. In lookup table-based DPC, the suitable switching states are selected from the switching table by minimizing the errors of active and reactive powers. However, one of the drawbacks of this approach is its varying switching frequency, which may result in broadband harmonic spectra [4], [8]–[10]. The passivity-based control (PBC) DPC [11], [12] and sliding mode control (SMC) [13], [14] approaches are presented to improve not only the transient but also the robust performance of the VSCs. However, the large ripple in both the active and reactive power are reported in the literature.

Recent developments in microprocessors and digital signal processors (DSPs) make the model predictive controller (MPC) an attractive control method for VSCs [15]–[17]. The first reason is that the MPC can control a great variety of complicated systems including delay, uncertainty, and/or disturbances. Even, the multivariable cases or the multi-input-multi-output systems can be easily investigated. Secondly, the hard constraints such as amplitude limitations on the input and output signals can be systematically considered through the MPC approach. Thirdly, in the case that the future reference signals are known, the MPC approach is extremely useful. Fourthly, because implementing the obtained control law and tuning the controller is relatively easy, thus it has a large amount of practical potential [18].

The MPC approach, which is used in the power electronics field, is divided into two categories named finite control set (FCS) MPC and continuous control set (CCS) MPC [19], [20]. In the FCS-MPC, the discrete nature of the VSCs is employed for designing the controller. In each iteration of the FCS-MPC, the cost function, which consists of current and prediction of the state variables, is evaluated for each possible switching state. Each switching state, which results in the optimal solution for the cost function, is implemented to the VSC [21]. However, if the number of the horizon is increased then the

complexity of the controller is increased. The two steps ahead prediction is suggested to avoid any computational delay in real-world applications [22]. The CCS-MPC needs a modulator to implement the controller to the VSCs, however, the FCS-MPC could directly provide the switching states for VSCs. Thus, the FCS-MPC may result in varying switching frequency, which consequently increases switching losses and broadband harmonic spectra, in the FCS-MPC approach. Additionally, varying switching frequency effects the steady-state performance of the VSCs [23]. There exist several types of CCS MPCs such as the nonlinear continuous-time MPC, which significantly improves the performance of the controlled system [24]. However, such complicated approaches usually result in large dynamical optimization problems, and nonconvex conditions. Furthermore, they require lots of computational effort and time. It is usually difficult to implement these kinds of MPC approaches in real-world applications. In the linear MPC method, the optimization algorithm can be restated as convex quadratic programming, which can be solved by the quadratic programming solvers. Additionally, linear MPC is well-known for its outstanding speed. Thus, the linear MPC technique has a more compatible structure over other complicated MPC approaches for the VSCs [25], [26]. According to the best knowledge of authors, experimental testing, designing constraint CCS-MPC and also optimal, simple unconstraint CCS-MPC for VSC have not been addressed in the literature, which are the main objectives of this manuscript.

In this paper, the problem of designing a constraint MPC and also an optimal unconstraint MPC have been investigated, separately. To do this, firstly, the dynamic model of the VSC is calculated. Secondly, the synchronous reference frame and the coordinate transfer are used to represent the state-space model in the dq frame. The obtained model is used to predict the future behavior of the VSC. Thirdly, the constraint and optimal unconstraint CCS-MPC for VSCs are proposed. In comparison with the state of art control approaches for VSCs, the proposed approach has the following advantages:

- Obtaining fix switching frequency for both constraint and unconstraint CCS-MPC.
- In unconstraint CCS-MPC, the optimal solution for the cost function will be obtained analytically.
- For constraint CCS-MPC, the nonconvex optimization problem is converted to a convex one. Then, the linear matrix inequality (LMI) is used to find the suboptimal solution for the convex optimization problem.
- Whereas the proposed design procedure is simple, the long horizon could be considered in the design procedure.

Finally, to evaluate the validity of the proposed approach, some experimental tests are extracted. Additionally, the better performance of the proposed approach is investigated by comparing the results with the state-of-the-art conventional control method.

The remaining part of this manuscript is organized as follows. The mathematical modeling of VSC is presented in Section II. Section III investigates the main results. The experimental testing is presented in Section IV. Finally, the paper is closed by conclusions in Section V.

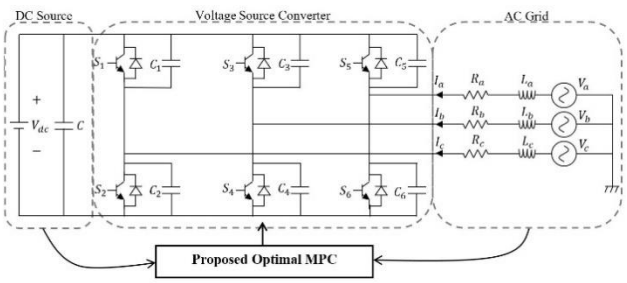

Fig. 1. Three-phase grid-connected VSC.

II. THE MATHEMATICAL MODEL OF VSC AND PRELIMINARIES

The state-space model of grid-connected VSC, presented in Figure 1, can be calculated as follows:

$$\begin{cases} L\dfrac{dI_a}{dt} = V_a - RI_a - \dfrac{2S_a - S_b - S_c}{3}V_{dc} \\ L\dfrac{dI_b}{dt} = V_b - RI_b - \dfrac{2S_b - S_a - S_c}{3}V_{dc} \\ L\dfrac{dI_c}{dt} = V_c - RI_c - \dfrac{2S_c - S_a - S_b}{3}V_{dc} \\ C\dfrac{dV_{dc}}{dt} = S_aI_a + S_bI_b + S_cI_c - \dfrac{V_{dc}}{R_L} \end{cases} \quad (1)$$

where V_a, V_b, and V_c are the three-phase voltages; I_a, I_b, and I_c denote the three-phase input current; The resistance and inductor of the three-phase AC filter are denoted by $R_a = R_b = R_C = R$, and $L_a = L_b = L_C = L$, respectively; V_{dc}, R_L, and C denote the output DC voltage, DC load, and capacitor, respectively; furthermore, the three-phase bridge is defined for the switching function in leg i (e.g. if S_a is 1, then S_1 is on and S_2 is off). By implementing the dq synchronous rotating coordinate, the equation (1) transfers to the following reduced dimensional model [27]:

$$\begin{cases} L\dfrac{dI_d}{dt} = V_d - RI_d + wLI_q - S_dV_{dc} \\ L\dfrac{dI_q}{dt} = V_q - RI_q - wLI_d - S_qV_{dc} \\ C\dfrac{dV_{dc}}{dt} = \dfrac{3}{2}\left(S_dI_d + S_qI_q\right) - \dfrac{V_{dc}}{R_L} \end{cases} \quad (2)$$

where the angular frequency of the input voltage is denoted by $w = 2\pi f$; V_d, V_q, I_d, and I_q denote the active, the reactive voltages, the active, and the reactive currents, respectively. The switching controllers in the dq structure is defined by S_d and S_q, which are bounded between zero and one.

III. MAIN RESULTS

By considering $S_{d_{eq}} = S_{q_{eq}} = 1$, the equilibrium point of (2) is obtained as follows:

$$\begin{cases} I_{q_{eq}} = \dfrac{\left(R + \frac{3}{2}R_L\right)V_q - \left(wL + \frac{3}{2}R_L\right)V_d}{R^2 + 3RR_L + w^2L^2} \\ I_{d_{eq}} = \dfrac{V_d}{R + \frac{3}{2}R_L} + \dfrac{wL - \frac{3}{2}R_L}{R + \frac{3}{2}R_L} \times I_{q_{eq}} \\ V_{dc_{eq}} = \dfrac{3}{2}R_L\left(I_{d_{eq}} + I_{q_{eq}}\right) \end{cases} \quad (3)$$

where $I_{d_{eq}}$, $I_{q_{eq}}$, and $V_{dc_{eq}}$ denote the equilibrium point of the nonlinear system (2). By linearizing the nonlinear system (2) around its equilibrium point, one has

$$\dot{x} = \begin{bmatrix} -\frac{R}{L} & w & -\frac{1}{L} \\ -w & -\frac{R}{L} & -\frac{1}{L} \\ \frac{3}{2C} & \frac{3}{2C} & -\frac{1}{CR_L} \end{bmatrix} x + \begin{bmatrix} -\frac{V_{dc_{eq}}}{L} & 0 \\ 0 & -\frac{V_{dc_{eq}}}{L} \\ \frac{3}{2C} I_{d_{eq}} & \frac{3}{2C} I_{q_{eq}} \end{bmatrix} u \quad (4)$$

where $x = [I_d \quad I_q \quad V_{dc}]^T$ and $u = [u_d \quad u_q]^T$. By employing the Euler discretization method, the discrete-time representation of the continuous-time system (4) can be calculated as follows:

$$\begin{cases} x(k+1) = Ax(k) + Bu(k) \\ y(k) = Cx(k) \end{cases} \quad (5)$$

where the matrices $A \in R^{3\times3}$, $B \in R^{3\times2}$, and $C \in R^{3\times3}$ are known constant system matrices. Consider the state-space model presented in (5). Then, the prediction of the output variables can be calculated as follows:

$$\begin{cases} y(k+1) = Cx(k+1) = CAx(k) + CBu(k) \\ y(k+2) = CAx(k+1) + CBu(k+1) \\ \quad = CA^2x(k) + CABu(k) + CBu(k+1) \\ y(k+3) = CA^2x(k+1) + CABu(k+1) + CBu(k+2) \\ y(k+N) = CA^Nx(k) + \sum_{j=1}^{N} CA^{N-j}Bu(k+j-1) \end{cases} \quad (6)$$

By deploying the predicted output presented in (5), the prediction $y(k)$ along the horizon N can be rewritten as follows:

$$Y(k) = Fx(k) + GU(k) \quad (7)$$

where

$$Y = \begin{bmatrix} y(k+1) \\ y(k+2) \\ \vdots \\ y(k+N) \end{bmatrix}, U = \begin{bmatrix} u(k) \\ u(k+1) \\ \vdots \\ u(k+N) \end{bmatrix}, F = \begin{bmatrix} CA \\ CA^2 \\ \vdots \\ CA^N \end{bmatrix}, \quad (8)$$

$$\text{and } G = \begin{bmatrix} CB & 0 & \cdots & 0 \\ CAB & CB & 0 & 0 \\ \vdots & \vdots & \ddots & \vdots \\ CA^{N-1}B & CA^{N-2}B & \cdots & CB \end{bmatrix}$$

Define the cost function:

$$J = \big(Y(k) - w(k)\big)^T P\big(Y(k) - w(k)\big) + U^T(k)QU(k) \quad (9)$$

where P and Q are known positive definite matrices and $w(k)$ denotes the reference signal. Next, two theorems will be provided. The first and second theorems design an MPC approach for the VSCs without and with constraints on the input and output variables, respectively.

Theorem 1 (unconstraint MPC) [28], [29]**.** *The optimal solution for the performance index (9) can be calculated using the Jacobian Hamilton optimization method as follows:*

$$\min_{U(k)} J \Rightarrow \; U(k) = (Q + G^TPG)^{-1}G^TP(W - Fx) \quad (10)$$

Then the first two rows of the control signal $U(k)$ is $u(k)$, which must be implemented to the system.

Proof: Substituting (7) into (9) results in

$$J = \big(Fx(k) + GU(k) - w(k)\big)^T P\big(Fx(k) + GU(k) - w(k)\big) + U^T(k)QU(k) \quad (11)$$

Minimizing the cost function (11) respect to $U(k)$, one has

$$\frac{\partial J}{\partial U} = G^TP\big(Fx(k) - W(k)\big) + (Q + G^TPG)U(k) = 0 \quad (12)$$

The proof is completed by simplifying equation (12). ■

Before investigating constraint MPC, the following lemma is introduced to convert the constraint MPC conditions to LMI ones.

Lemma 1 (Schur complement) [30], [31]**.** *Consider an affine function F, which is partitioned as follows:*

$$F = \begin{bmatrix} F_{11} & F_{12} \\ F_{21} & F_{22} \end{bmatrix}$$

Then, $F < 0$ is satisfied if and only if one of the following inequalities are satisfied:

$$\begin{cases} F_{11} < 0 \\ F_{22} - F_{21}F_{11}^{-1}F_{12} < 0 \end{cases} \quad (13)$$

or

$$\begin{cases} F_{22} < 0 \\ F_{11} - F_{12}F_{22}^{-1}F_{21} < 0 \end{cases} \quad (14)$$

Theorem 2 (constraint MPC). *The suboptimal solution for the cost function (9) is obtained if there exists any matrix $U(k)$ such that the following linear matrix inequalities (LMIs) are satisfied:*

Minimize γ subject to

$$\begin{bmatrix} H_{11}(k) & U^T(k) \\ U(k) & -(Q + G^TPG) \end{bmatrix} < 0 \quad (15)$$

$$diag\{U - U_{max}\} < 0 \quad (16)$$

$$diag\{U - U_{min}\} > 0 \quad (17)$$

$$diag\{Fx(k) + GU(k) - Y_{max}\} < 0 \quad (18)$$

$$diag\{Fx(k) + GU(k) - Y_{min}\} > 0 \quad (19)$$

where $H_{11}(k) = \big(Fx(k) - w(k)\big)^T P\big(Fx(k) - w(k)\big) + U^T(k)G^TP\big(Fx(k) - w(k)\big) + \big(Fx(k) - w(k)\big)^T PGU(k) - \gamma$, *and $u(k)$ is the first m entries rows of matrix U. Furthermore, the obtained control signal makes the output of the system track the reference with the performance index γ. Additionally, the amplitudes of the control and output signals are assumed to be inside a predefined region by defining U_{max}, U_{min}, Y_{max}, and Y_{min}.*

Proof: Equations (16) and (17) address the constraints on the amplitude of the input signal. Consider (*7*), then the constraints on the amplitude of the output signals can be introduce by (18) and (19). Now, we would like to minimize the cost function (9) such that constraints (16), (17), (18), and (19) are satisfied. Due to inequality constraints, the numerical algorithm is required to solve the optimization problem. To minimize the cost function (9), the following equivalent minimization problem is considered:

$$\big(Y(k) - w(k)\big)^T P\big(Y(k) - w(k)\big) + U^T(k)QU(k) < \gamma \quad (20)$$

where $\gamma > 0$ is the performance level, which will be minimized through the optimization process. Substituting (7) into (*20*) results in

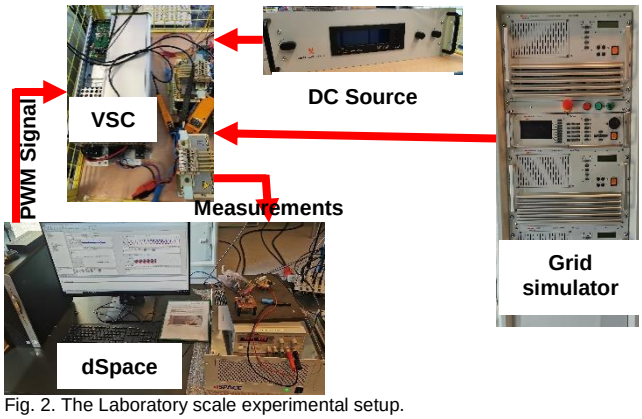

Fig. 2. The Laboratory scale experimental setup.

$$\big(Fx(k)+GU(k)-w(k)\big)^T P\big(Fx(k)+GU(k) - w(k)\big)+U^T(k)QU(k)<\gamma \quad (21)$$

Equation (*21*) can be rewritten as follows:

$$\begin{aligned}&\big(Fx(k)+GU(k)-w(k)\big)^T P\big(Fx(k)-w(k)\big)\\&+\big(Fx(k)-w(k)\big)^T PGU(k)\\&-\gamma+U^T(k)[Q+G^T PG]U(k)\\&<0\end{aligned} \quad (22)$$

The proof is completed by utilizing the Schur complement. ■

IV. Experimental Testing

To evaluate the validity and the better performance of the proposed approach, some experimental tests are performed. The laboratory-scale testbed setup is shown in Fig. 2. The setup comprises a DC source, a three-phase VSC, a three-phase SPITZENBERGER SPIES supply grid simulator, and a three-phase series resistor R and inductor L. In this experiment, the three-phase inductor and resistor are considered to be 4.4 mH and 0.5Ω, respectively. The 4.4 mH is obtained from the series connection of two separate inductors with the value of 2.2 mH. The DC voltage is set to be 500 V. The grid simulator provides the three-phase AC voltage with the amplitude of 120 V. The proposed controller is simulated in MATLAB Simulink and implemented to the laboratory scale testbed setup using dSPACE. To do this, a personal Core i7, 2.11 GHz, and 16GB RAM computer is used. The dSPACE setup consists of a compact set of a DS I/O board, a Semikron Power Electronic Teaching Unit, and a Micro Lab Box DC Power. Boards DS2004 and the board DS5101 are used as a high-speed analog to digital converter and pulse width modulator (PWM) waveform generator, respectively.

To evaluate the validity of the proposed approaches, Theorem 1 is simulated in MATLAB simulink and implemented to the dSPACE. Then the proposed controller is experimentally tested and compared with the conventional PI controller. Fig. 3. and Fig. 4. illustrate the behavior of the VSC for the proposed approach and PI controller, respectively. Fig. 3. and Fig. 4. are obtained from the dSPACE control desk. In Fig. 3. and Fig. 4., the red lines show the active current and the blue ones indicate the reactive current. Based on Fig. 3. and Fig. 4., the proposed approach provides better transient performance in comparison with the conventional PI controller. In this case, not only the settling time but also the percentage of overshoot is decreased in the CCS-MPC technique. The reason is that tuning the PI controller parameters needs significant effort, and the PI controller can

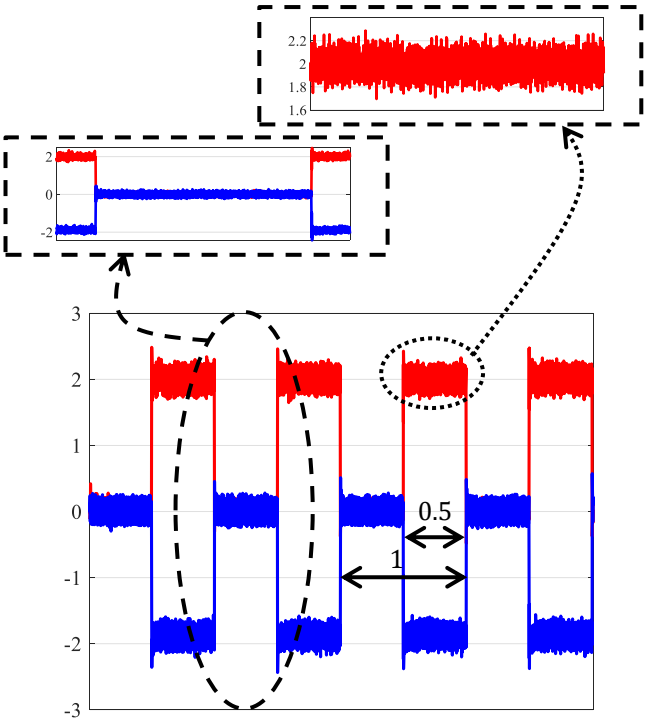

Fig. 3. The active and reactive response of the VSC for the prosed CCS-MPC. The red and blue lines indicate the active and the reactive currents, respectively.

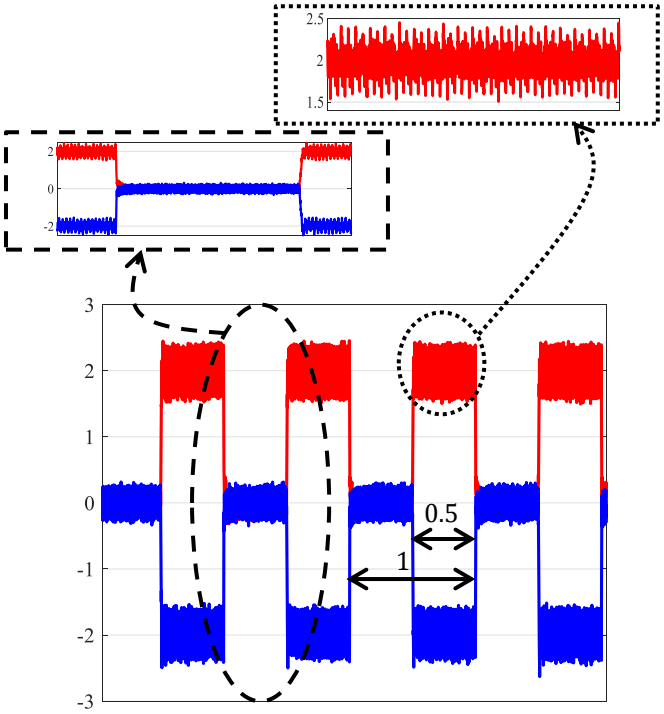

Fig. 4. The active and reactive response of the VSC for the PI controller. The red and blue lines indicate the active and the reactive currents, respectively.

not reduce the settling time and percentage of overshoot simultaneously. However, the proposed approach provides a framework to control the percentage of the overshoot besides the settling time. Additionally, the switching effect on the proposed approach is less than the one that appeared in the

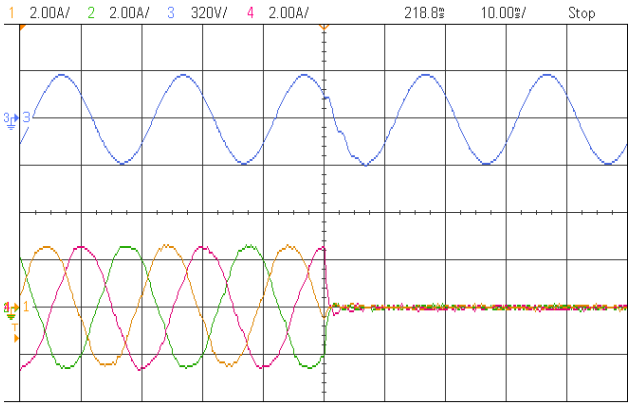

Fig. 5. Experimental validation for the proposed optimal CCS-MPC approach. The ac voltage of one of the three-phase is illustrated by the blue line and the three-phase current is shown by red, green, and yellow colors.

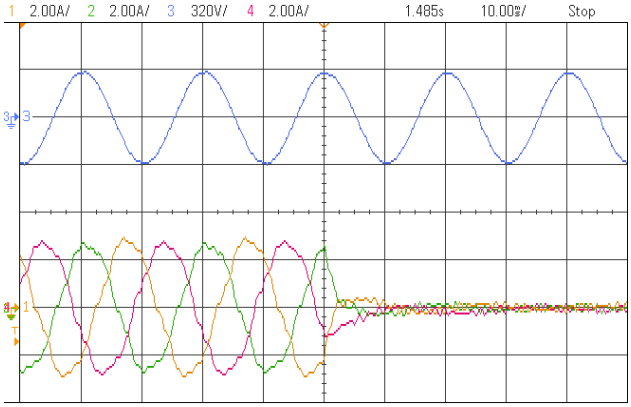

Fig. 6. Experimental validation for the PI controller. The ac voltage of one of the three-phase is illustrated by the blue line and the three-phase current is shown by red, green, and yellow colors.

conventional PI controller. Fig. 5 and Fig. 6 illustrate the three-phase signals for the proposed approach and conventional PI controller, respectively. The controlled three-phase current of the VSC is illustrated by red, green, and yellow colors and the voltage of one of the three phases is shown by blue color. As shown in Fig. 5 the percentage of the overshoot and the settling time of the proposed approach is significantly better than the PI controller, presented in Fig. 6. Additionally, the steady-state performance of the proposed approach is better than the PI controller. The reason is that the switching effect in the proposed approach is less than the switching effect in the PI controller.

V. Conclusions

In this paper, a reliable CCS-MPC was proposed to improve the transient performance of the VSC. Two types of unconstraint and constraint CCS-MPC approaches were investigated in this paper. For the unconstraint MPC approach, the optimal solution was analytically calculated. Because the constraint CCS-MPC was not analytically solvable, sufficient conditions to guarantee the performance of the VSC were obtained in terms of LMIs. Then, the Yalmip toolbox, which is a convex optimization method, in MATLAB was used to find the suboptimal solution. Generally, the advantages of the proposed approach were constant switching frequency, fast transient performance in terms of settling time and percentage of overshoot, and hard constraints on the input and output signals, which were the control and the currents signals of the converters. By using dSPACE, the proposed unconstraint CCS-MPC was implemented on the laboratory scale testbed setup. Experimental results indicate the better performance of the proposed approach in comparison with the conventional PI controller. From the experimental results, one can conclude that the injected and consumed powers for the proposed approach are more balanced compared with the state-of-the-art control method. Furthermore, it became apparent that the responses of the proposed approach were faster in terms of settling time and percentage of overshoot than the conventional PI controller.

References

[1] J. Liu, X. Tao, M. Yu, Y. Xia, and W. Wei, "Impedance Modeling and Analysis of Three-Phase Voltage-Source Converters Viewing From DC Side," *IEEE J. Emerg. Sel. Top. Power Electron.*, vol. 8, no. 4, pp. 3906–3916, Dec. 2020, doi: 10.1109/JESTPE.2019.2932618.

[2] M. S. O. Yeganeh, P. Davari, A. Chub, N. Mijatovic, T. Dragičević, and F. Blaabjerg, "A Single-Phase Reduced Component Count Asymmetrical Multilevel Inverter Topology," *IEEE J. Emerg. Sel. Top. Power Electron.*, pp. 1–1, 2021, doi: 10.1109/JESTPE.2021.3066396.

[3] M. G. Taul, X. Wang, P. Davari, and F. Blaabjerg, "An Overview of Assessment Methods for Synchronization Stability of Grid-Connected Converters Under Severe Symmetrical Grid Faults," *IEEE Trans. Power Electron.*, vol. 34, no. 10, pp. 9655–9670, Oct. 2019, doi: 10.1109/TPEL.2019.2892142.

[4] Y. Gui, X. Wang, F. Blaabjerg, and D. Pan, "Control of Grid-Connected Voltage-Source Converters: The Relationship Between Direct-Power Control and Vector-Current Control," *IEEE Ind. Electron. Mag.*, vol. 13, no. 2, pp. 31–40, Jun. 2019, doi: 10.1109/MIE.2019.2898012.

[5] K. Sun, W. Yao, J. Fang, X. Ai, J. Wen, and S. Cheng, "Impedance Modeling and Stability Analysis of Grid-Connected DFIG-Based Wind Farm With a VSC-HVDC," *IEEE J. Emerg. Sel. Top. Power Electron.*, vol. 8, no. 2, pp. 1375–1390, Jun. 2020, doi: 10.1109/JESTPE.2019.2901747.

[6] D. N. Zmood and D. G. Holmes, "Stationary frame current regulation of PWM inverters with zero steady-state error," *IEEE Trans. Power Electron.*, vol. 18, no. 3, pp. 814–822, May 2003, doi: 10.1109/TPEL.2003.810852.

[7] S. Gao, H. Zhao, Y. Gui, J. Luo, and F. Blaabjerg, "Impedance Analysis of Voltage Source Converter Using Direct Power Control," *IEEE Trans. Energy Convers.*, pp. 1–1, 2020, doi: 10.1109/TEC.2020.3020181.

[8] G. Escobar, A. M. Stankovic, J. M. Carrasco, E. Galvan, and R. Ortega, "Analysis and design of direct power control (DPC) for a three phase synchronous rectifier via output regulation subspaces," *IEEE Trans. Power Electron.*, vol. 18, no. 3, pp. 823–830, May 2003, doi: 10.1109/TPEL.2003.810862.

[9] M. S. O. Yeganeh, M. Sarvi, F. Blaabjerg, and P. Davari, "Improved harmonic injection pulse-width modulation variable frequency triangular carrier scheme for multilevel inverters," *IET Power Electron.*, vol. 13, no. 14, pp. 3146–3154, 2020, doi: 10.1049/iet-pel.2020.0232.

[10] M. S. O. Yegane and M. Sarvi, "A New Improved Variable Frequency Triangular Carrier-PWM with MOPSO Algorithm for Carrier Based PWM Techniques in Inverters," *TEM J.*, vol. 6, no. 1, pp. 32–42, 2017.

[11] D. del Puerto-Flores, J. M. A. Scherpen, M. Liserre, M. M. J. de Vries, M. J. Kransse, and V. G. Monopoli, "Passivity-Based Control by Series/Parallel Damping of Single-Phase PWM Voltage Source Converter," *IEEE Trans. Control Syst. Technol.*, vol. 22, no. 4, pp. 1310–1322, Jul. 2014, doi: 10.1109/TCST.2013.2278781.

[12] A. J. Agbemuko, J. L. Domínguez-García, O. Gomis-Bellmunt, and L. Harnefors, "Passivity-Based Analysis and Performance Enhancement of a Vector Controlled VSC Connected to a Weak AC Grid," *IEEE Trans. Power Deliv.*, vol. 36, no. 1, pp. 156–167, Feb. 2021, doi: 10.1109/TPWRD.2020.2982498.

[13] H. Komurcugil, S. Biricik, S. Bayhan, and Z. Zhang, "Sliding Mode Control: Overview of Its Applications in Power Converters," *IEEE Ind. Electron. Mag.*, pp. 0–0, 2020, doi: 10.1109/MIE.2020.2986165.

[14] C. Lascu, "Sliding Mode Direct Voltage Control of Voltage Source Converters with LC Filters for Pulsed Power Loads," *IEEE Trans. Ind. Electron.*, pp. 1–1, 2020, doi: 10.1109/TIE.2020.3040694.

[15] M. Novak, U. M. Nyman, T. Dragicevic, and F. Blaabjerg, "Statistical Model Checking for Finite-Set Model Predictive Control Converters: A Tutorial on Modeling and Performance Verification," *IEEE Ind. Electron. Mag.*, vol. 13, no. 3, pp. 6–15, Sep. 2019, doi: 10.1109/MIE.2019.2916232.

[16] H. A. Young, M. A. Perez, J. Rodriguez, and H. Abu-Rub, "Assessing Finite-Control-Set Model Predictive Control: A Comparison with a Linear Current Controller in Two-Level Voltage Source Inverters," *IEEE Ind. Electron. Mag.*, vol. 8, no. 1, pp. 44–52, Mar. 2014, doi: 10.1109/MIE.2013.2294870.

[17] T. Dragičević, "Model Predictive Control of Power Converters for Robust and Fast Operation of AC Microgrids," *IEEE Trans. Power Electron.*, vol. 33, no. 7, pp. 6304–6317, Jul. 2018, doi: 10.1109/TPEL.2017.2744986.

[18] E. F. Camacho and C. B. Alba, *Model Predictive Control*, 2nd ed. London: Springer-Verlag, 2007. doi: 10.1007/978-0-85729-398-5.

[19] Z. Zhao *et al.*, "Decentralized Finite Control Set Model Predictive Control Strategy of Microgrids for Unbalanced and Harmonic Power Management," *IEEE Access*, vol. 8, pp. 202298–202311, 2020, doi: 10.1109/ACCESS.2020.3034947.

[20] A. A. Ahmed, B. K. Koh, and Y. I. Lee, "A Comparison of Finite Control Set and Continuous Control Set Model Predictive Control Schemes for Speed Control of Induction Motors," *IEEE Trans. Ind. Inform.*, vol. 14, no. 4, pp. 1334–1346, Apr. 2018, doi: 10.1109/TII.2017.2758393.

[21] S. Vazquez *et al.*, "Model Predictive Control: A Review of Its Applications in Power Electronics," *IEEE Ind. Electron. Mag.*, vol. 8, no. 1, pp. 16–31, Mar. 2014, doi: 10.1109/MIE.2013.2290138.

[22] P. Cortes, J. Rodriguez, C. Silva, and A. Flores, "Delay Compensation in Model Predictive Current Control of a Three-Phase Inverter," *IEEE Trans. Ind. Electron.*, vol. 59, no. 2, pp. 1323–1325, Feb. 2012, doi: 10.1109/TIE.2011.2157284.

[23] S. Vazquez *et al.*, "Model Predictive Control for Single-Phase NPC Converters Based on Optimal Switching Sequences," *IEEE Trans. Ind. Electron.*, vol. 63, no. 12, pp. 7533–7541, Dec. 2016, doi: 10.1109/TIE.2016.2594227.

[24] L. Wang, *Model Predictive Control System Design and Implementation Using MATLAB®*. London: Springer, 2009.

[25] J.-H. Lee and K.-B. Lee, "A Dead-Beat Control for Bridgeless Inverter Systems to Reduce the Distortion of Grid Current," *IEEE J. Emerg. Sel. Top. Power Electron.*, vol. 6, no. 1, pp. 151–164, Mar. 2018.

[26] R. Findeisen and F. Allgöwer, "An Introduction to Nonlinear Model Predictive Control," in *21st Benelux Meeting on Systems and Control, Veidhoven*, 2002, pp. 1–23.

[27] X. Guo, H. Ren, and J. Li, "Robust Model-Predictive Control for a Compound Active-Clamp Three-Phase Soft-Switching PFC Converter Under Unbalanced Grid Condition," *IEEE Trans. Ind. Electron.*, vol. 65, no. 3, pp. 2156–2166, Mar. 2018, doi: 10.1109/TIE.2017.2745474.

[28] M. M. Mardani, M. H. Khooban, A. Masoudian, and T. Dragičević, "Model Predictive Control of DC–DC Converters to Mitigate the Effects of Pulsed Power Loads in Naval DC Microgrids," *IEEE Trans. Ind. Electron.*, vol. 66, no. 7, pp. 5676–5685, Jul. 2019, doi: 10.1109/TIE.2018.2877191.

[29] N. Vafamand, M. M. Mardani, M. H. Khooban, F. Blaabjerg, and J. Boudjadar, "Pulsed power load effect mitigation in DC shipboard microgrids: a constrained modelpredictive approach," *IET Power Electron.*, vol. 12, no. 9, pp. 2155–2160, 2019, doi: 10.1049/iet-pel.2018.6159.

[30] C. Scherer and W. Siep, *Linear matrix inequalities in control*, vol. 3. Lecture Notes, Dutch Institute for Systems and Control, Delft, The Netherlands, 2000.

[31] M. M. Mardani, N. Vafamand, M. H. Khooban, T. Dragicevic, and F. Blaabjerg, "Non-fragile controller design of uncertain saturated polynomial fuzzy systems subjected to persistent bounded disturbance," *Trans. Inst. Meas. Control*, vol. 41, no. 3, pp. 842–858, Feb. 2019, doi: 10.1177/0142331218774110.